

---

# Novel Phonoreceptive Mechanism of the Cochlear for Low-frequency Sound

W. Yao,<sup>1,\*</sup> J. Ma,<sup>1</sup> J. Liang,<sup>2</sup> X. Huang,<sup>3</sup> and Y. Chen<sup>1</sup>

<sup>1</sup>Shanghai Institute of Applied Mathematics and Mechanics, Shanghai 200072, PRC

<sup>2</sup>University of Maryland School of Medicine, Baltimore, Maryland 21201, USA

<sup>3</sup>Department of Otorhinolaryngology, Zhongshan Hospital, Fudan University, Shanghai 200032, PRC

\*Corresponding author, Correspondence and requests for materials should be addressed to W. Yao.  
(email: wjyao@shu.edu.cn).

Nobel Laureate von Békésy experimentally discovered travelling wave vibration of the basilar membrane (BM) in the cochlear, which first reveals the motion law of the crucial structure of human phonoreceptive mechanism. However, with the further development of research, many scientists have discovered that the travelling wave vibration unable to explain many experimental observations and the low-frequency hearing of the cochlear. Because the cochlear is very small and complex, vibration data of the whole BM are not yet available from existing experiments, and low-frequency vibration data are absent from Békésy's and other experiments. To address this question, this work technically adopts the transformation tensor mapping relation to established a theoretical analytical model of the Spiral cochlear based on the theory of physics and biology, combined with medical and modern light source imaging experimental data. In addition, a numerical model of a real human ear is also established. By performing numerous calculation, the results reproduce the known travelling wave vibration of BM. Meanwhile, an exciting finding that revealing a new standing wave vibration mode at low frequencies is obtained. More importantly, this newly discovered model intrinsically explain many experimental observations that cannot be explained by travelling wave theory, which solves a long standing various queries to travelling wave vibration among researchers. These results not only complement low-frequency vibration data that are inaccessible through experiments but also reveal a new hearing mechanism.

This paper carries out a systematic research including comparative analysis of analytical solution, numerical simulation with experimental results.

The cochlear is an important functional structure in the auditory pathway (Fig. 1), for there is a fundamental structure called basilar membrane (BM) which plays a key role for human hearing sensation [1].

The investigation of phonoreceptive mechanism of human cochlear is a major medical problem for mankind. It has received wide attention from many life scientists and medical works [2]. Up to now, scientists have not reached a consensus on the vibrating mode of the key macrostructure--basilar membrane. The achievement of auditory function in the cochlear is attributed to fluid-structure coupling motions between lymph and BM. Revealing the kinetics of BM in the lymph of cochlear is a primary and pivotal question to understanding phonoreceptive mechanism of human cochlear [3].

Regarding this crucial question, Békésy in 1960 proposed his famous traveling wave theory [4] by measuring the motions of the BM from fresh temporal bones, for which he was awarded a Nobel prize. From then on, numerous researchers have proposed

mathematical and mechanical models [5-10] to describe the observed vibration behavior of the BM based on the traveling wave theory. But with the progress of research in this field, many scientists have raised doubts about the traveling wave theory since the end of last century, doubts originating from the nonviability of traveling wave theory in explaining many experimental discoveries and low-frequency sound hearing of the cochlear [11-14], as Békésy's experimental data did not include the data of BM vibration of cochlea at low frequencies.

It is worth mentioning that it is generally believed that the low-frequency hearing ability is attributed to the apical mechanical behavior of the BM [15-16]. However, it is so difficult to obtain the coupling biological dynamic process between BM and lymph in low-frequency via vivo experiments. In particular, because the apical space is narrow and with complex structures, mechanical responses at the apex of the BM are still poorly understood since no such data have been obtained from cochlear that were reasonably free of experimenter-induced damage. The method for measuring cochlear vibrations requires the placement of artifacts on the vibrating structures and, therefore, often perforating Reissner's membrane [17], which

destroy physiologically environment in the cochlea and affect the system motion mechanism [15]. Meanwhile, there are no experimental measurements of the BM vibration in low-frequency so far.

In view of above problems, based upon our decade spanning endeavor in the field of biomechanical investigation of human ear, this work first technically adopts the transformation tensor mapping relation to established a three-dimensional spiral cochlear fluid-structure mechanical analytical model. Meanwhile, in order to make our research more accurate and credible, a most physiologically accurate human ear numerical simulation model is established, based on the most advanced CT imaging technology in Shanghai Synchrotron Radiation Facility and then the real geometrical data of the human ear (including outer ear, middle ear and inner ear) was obtained. In addition, this model was completely in line with morphology of human ears, physiological environment and properties of biological materials. This accurate analytical model and the numerical model characterized by above remarkable features have not been reported in past works.

The presented analytical solutions and numerical simulation results predict the displacement amplitude of BM in low frequencies that cannot be measured in the experiment. A new and exciting discovery is found that there exists a new kind of wave, that is standing wave, which is notably distributed on the BM in low frequencies. This finding has not been reported so far and cannot be measured via present experimental technology. More importantly, the standing wave vibration can explain the experimental phenomena which are unexplainable by the travelling wave theory, thus giving an answer to the questions of many scientists about the traveling wave theory for many years.

The cochlear fluid is generally treated to be incompressible and inviscid [4-5,14]. As such, the Laplace equation is given by:

$$\nabla^2 \Phi(s, n, \xi) = 0 \quad (1)$$

where  $\nabla^2$  is the Laplace operator in the curvilinear coordinates. Since we obtain the mapping tensor  $\mathbf{G}$  from  $(x, y, z)$  to  $(s, n, \xi)$ ,  $\mathbf{G}^{-1}$  denotes the mapping tensor from the curvilinear coordinates  $(s, n, \xi)$  to rectangular coordinates  $(x, y, z)$ . Based on the variation method, we deduce the Laplace operator  $\nabla^2$  in the curvilinear coordinates. The Einstein's summation convention has been used and the Laplacian takes the form:

$$\nabla^2 = \frac{1}{|G|} \frac{\partial}{\partial x^i} \left( \sqrt{|G|} (G^{-1})^{ij} \frac{\partial}{\partial x^j} \right), \quad (x^1 = s, x^2 = n, x^3 = \xi) \quad (2)$$

where  $|G|$  represents the determinant of  $\mathbf{G}$

(The derivation process of  $\mathbf{G}$  is shown in **Supplemental Material** in detail),  $(G^{-1})^{ij}$  denote the element in Row  $i$ th Column  $j$ th of the mapping tensor from the curvilinear coordinates to rectangular coordinates. Substitute Eq. (2) into Eq. (1), we obtain:

$$\begin{aligned} & (1-\kappa n) \frac{\partial^2 \Phi}{\partial s^2} + \left[ (1-\kappa n)^3 + (1-\kappa n) \tau^2 \xi^2 \right] \frac{\partial^2 \Phi}{\partial n^2} + (\kappa \tau^2 \xi^2 + \tau \xi \kappa' n) \frac{\partial \Phi}{\partial n} \\ & + \left[ (1-\kappa n)^3 + (1-\kappa n) \tau^2 n^2 \right] \frac{\partial^2 \Phi}{\partial \xi^2} + \left[ (\kappa' n + \kappa \tau \xi) - \tau' n (1-\kappa n) \right] \frac{\partial \Phi}{\partial s} \\ & + \left[ \tau' \xi (1-\kappa n) - \tau^2 n (1-\kappa n) - \kappa (1-\kappa n)^2 + \kappa \tau^2 \xi^2 + \tau \xi \kappa' n \right] \frac{\partial \Phi}{\partial n} \\ & + 2(1-\kappa n) \left[ \tau \xi \frac{\partial^2 \Phi}{\partial s \partial n} - \tau n \frac{\partial^2 \Phi}{\partial s \partial \xi} + \tau^2 n \xi \frac{\partial^3 \Phi}{\partial n \partial \xi} \right] = 0 \end{aligned} \quad (3)$$

where  $\Phi(s, n, \xi)$  is the fluid velocity potential function.  $\kappa$  and  $\tau$  are curvature and torsion of BM respectively (The derivation of  $\kappa$  and  $\tau$  are shown in **Supplemental Material** in detail). When  $\tau = 0$ , the formulation can return to that describes the cochlear cavity rotating on the same surface around the cochlear axis. Herein, the Laplace equation of fluid can be simplified as:

$$(1-\kappa n) \frac{\partial^2 \Phi}{\partial s^2} + (1-\kappa n)^3 \frac{\partial^2 \Phi}{\partial n^2} + (1-\kappa n)^3 \frac{\partial^2 \Phi}{\partial \xi^2} - \kappa (1-\kappa n)^2 \frac{\partial \Phi}{\partial n} + \kappa' n \frac{\partial \Phi}{\partial s} = 0 \quad (4)$$

and gives

$$\begin{aligned} \dot{u} &= \sqrt{(G^{-1})^{11}} \frac{\partial \Phi}{\partial s} + \sqrt{(G^{-1})^{21}} \frac{\partial \Phi}{\partial n} + \sqrt{(G^{-1})^{31}} \frac{\partial \Phi}{\partial \xi} \\ \dot{v} &= \sqrt{(G^{-1})^{12}} \frac{\partial \Phi}{\partial s} + \sqrt{(G^{-1})^{22}} \frac{\partial \Phi}{\partial n} + \sqrt{(G^{-1})^{32}} \frac{\partial \Phi}{\partial \xi} \\ \dot{w} &= \sqrt{(G^{-1})^{13}} \frac{\partial \Phi}{\partial s} + \sqrt{(G^{-1})^{23}} \frac{\partial \Phi}{\partial n} + \sqrt{(G^{-1})^{33}} \frac{\partial \Phi}{\partial \xi} \end{aligned} \quad (5)$$

where  $u, w, v$  are displacement components of fluid along  $s, n, \xi$  respectively. And dot denotes differentiation with respect to time. For Eq. (5), assuming that  $\vec{n}_1, \vec{n}_2$  are unit normal vectors respectively along the inner boundary and outer boundary, and  $\vec{n}_u, \vec{n}_l$  are unit normal vectors of upper boundary and lower boundary. The fixed external boundary of cochlear cavity has a zero flux, then gives:

$$\begin{aligned} \frac{\partial \Phi}{\partial n_i} = \vec{n}_i \cdot \nabla \Phi = 0, \quad i = 1, 2 \quad \frac{\partial \Phi}{\partial n_u} = \vec{n}_u \cdot \nabla \Phi = 0 \\ \frac{\partial \Phi}{\partial n_l} = \vec{n}_l \cdot \nabla \Phi = 0 \end{aligned} \quad (6)$$

In addition, at the interface of the fluid and BM, the velocity of fluid and BM remain the same, and gives:

$$\frac{\partial \Phi}{\partial n_i} = \vec{n}_i \cdot \nabla \Phi = -\frac{\partial}{\partial t} W(s, n, \pm h/2, t) \quad (7)$$

where  $W$  represents the BM vertical displacement that perpendicular to the central plane of the cochlear. Because there are no vertical displacement in spiral lamina that adjoins the two sides of BM, based on the

variation principle, the BM displacement should be a sine form, expressed by:

$$w_p(s, n, t) = W \sin^2 \left[ \frac{\pi(n + b_{BM}/2)}{b_{BM}} \right] e^{i\varphi} \quad (8)$$

Furthermore, the phase  $\varphi$  is given by:

$$\varphi = \omega t - \lambda s \quad (9)$$

where  $\omega$  denotes frequency,  $\lambda$  is wavenumber. The solution which satisfies the first two conditions of Eq. (6) is :

$$\Phi = \sum_{j=0}^{\infty} B_j \cosh m_j (\xi - H) \cos \left[ j\pi \left( n + \frac{b}{2} \right) / b \right] e^{i\varphi} \quad (10)$$

where  $B_j, m_j$  can be obtained through Eq. (6). It should be noted that  $B_j, m_j$  are both function of the curvature and torsion. Once the  $\Phi$  is determined, the fluid pressure can be obtained by N-S equation:

$$p = -\rho \frac{\partial \Phi}{\partial t} \quad (11)$$

where  $\rho$  is the fluid density,  $p$  is the fluid pressure. The nonlinear terms can be ignored when compared with the linear term.

In order to derive the  $\bar{n} \cdot \nabla$  term of the boundary conditions of fluid, using the following expression:

$$\bar{n} \cdot \nabla = G^{-1} N_p \frac{\partial}{\partial u^q} \quad (12)$$

Herein, define  $\left\{ \bar{E}_s, \bar{E}_n, \bar{E}_\zeta \right\}$  as contravariant vector, that is, the unit normal vector of the fixed coordinates. In the above, the  $G^{-1}$  term in Eq. (12) has been determined. Thus,  $N_p$  term is only needed to determine the normal directional derivative. Let  $F_1(n, s) = n - n_1(s) = 0$ , the normal vector of the inner boundary of cochlear can be expressed as:

$$\bar{n}_1 = -K_1 \nabla F_1 = -K_1 (\bar{E}_n - n'_1 \bar{E}_s) \quad (13)$$

where  $K_1$  is scaling factor which makes  $n_1 \cdot n_1 = 1$ . Through the expression of scalar product tensor  $n_1 \cdot n_1 = G^{-1} n_{1p} n_{1q}$ , it gives:

$$\bar{n}_1 = \frac{-1}{\sqrt{1 + \frac{n'^2}{n^2}}} (\bar{E}_n - n'_1 \bar{E}_s) \quad (14)$$

and then gives:

$$\bar{n}_1 \cdot \nabla = G^{-1} N_p \frac{\partial}{\partial u^q} = \frac{-1}{\sqrt{1 + \frac{n'^2}{n^2}}} \left\{ \frac{\partial}{\partial n} + \frac{n'_1}{n^2} \left( -\frac{\partial}{\partial s} + \kappa \frac{\partial}{\partial \zeta} \right) \right\} \quad (15)$$

Similarly, the normal directional derivative of outer boundary of cochlear can be derived as:

For previous cochlear models, the WKB

$$\bar{n}_2 \cdot \nabla = G^{-1} N_p \frac{\partial}{\partial u^q} = \frac{-1}{\sqrt{1 + \frac{n_2'^2}{n^2}}} \left\{ \frac{\partial}{\partial n} + \frac{n_2'}{n^2} \left( -\frac{\partial}{\partial s} + \kappa \frac{\partial}{\partial \zeta} \right) \right\} \quad (16)$$

Let  $F_u(s, \zeta) = \zeta - h(s) = 0$ ,  $F_l(s, \zeta) = \zeta = 0$ , the normal derivative of upper boundary and lower boundary can be expressed as:

$$\bar{n}_u = K_u \nabla F_u = K_u (-h' \bar{E}_s + \bar{E}_\zeta) \quad (17)$$

$$\bar{n}_l = -K_l \nabla F_l = -K_l \bar{E}_\zeta$$

where

$$K_u = \frac{1}{\sqrt{1 + \left( \frac{\kappa + h'}{n} \right)^2}}, K_l = \frac{1}{\sqrt{1 + \left( \frac{\kappa}{n} \right)^2}} \quad (18)$$

According to above equation, the normal directional derivative of upper boundary can be written as:

$$\bar{n}_u \cdot \nabla = G^{-1} N_p \frac{\partial}{\partial u^q} = \frac{1}{\sqrt{1 + \left( \frac{\kappa + h'}{n} \right)^2}} \left[ \left( \frac{h' + \kappa}{n^2} \right) \frac{\partial}{\partial s} + \left( 1 + \frac{\kappa(\kappa + h')}{n^2} \right) \frac{\partial}{\partial \zeta} \right] \quad (19)$$

The normal directional derivative of lower boundary can be written as:

$$\bar{n}_l \cdot \nabla = G^{-1} N_p \frac{\partial}{\partial u^q} = \frac{1}{\sqrt{1 + \left( \frac{\kappa}{n} \right)^2}} \left[ -\left( \frac{\kappa}{n^2} \right) \frac{\partial}{\partial s} + \left( 1 + \frac{\kappa^2}{n^2} \right) \frac{\partial}{\partial \zeta} \right] \quad (20)$$

The BM is regarded as a isotropic thin plate and the vibration control equation can be written as:

$$h \left( 1 - \frac{h^2 \tau^2}{12} \right) \left( m \frac{\partial^2}{\partial t^2} + \beta \frac{\partial}{\partial t} \right) w_p + D \left( \frac{\partial^2}{\partial n^2} - 2\tau^2 \right) \left( \frac{\partial^2}{\partial n^2} + \tau^2 \right) w_p = (1 - h^2 \tau^2 / 4) \left( [\sigma^{33}]^+ + [\sigma^{33}]^- \right) - hf \left( [\sigma^{33}]^+ - [\sigma^{33}]^- \right) / 2 \quad (21)$$

where  $\sigma^{33}$  denotes the Row 3 and Column 3 element of second order Piola-Kirchoff stress tensor,  $m$  denotes the mass density of BM,  $\beta$  denotes the damping of BM, and  $f$  denotes the function of BM curvature and torsion. Only the BM motion in  $\zeta$  axis is considered, the kinetic energy is:

$$T_p = \int_{-\frac{b_{BM}}{2}}^{\frac{b_{BM}}{2}} \frac{1}{2\pi} \int_0^{2\pi} \frac{1}{2} \rho_p h w_p^2 d\varphi dn \quad (22)$$

where  $\rho_p$  is the density of BM. Substitute Eq. (8) into Eq. (22), it yields

$$T_p = \frac{1}{4} \rho_p \omega^2 h W^2 \int_{-\frac{b_{BM}}{2}}^{\frac{b_{BM}}{2}} \eta^2(n) dn \quad (23)$$

For a homogeneous, isotropic plate, the averaged potential energy is:

$$V = \int_{-\frac{b_{BM}}{2}}^{\frac{b_{BM}}{2}} \frac{1}{2\pi} \int_0^{2\pi} \frac{D}{2} \left[ \left( \frac{\partial^2 w_p}{\partial s^2} \right)^2 + \left( \frac{\partial^2 w_p}{\partial n^2} \right)^2 + 2\nu \left( \frac{\partial^2 w_p}{\partial s^2} \right) \left( \frac{\partial^2 w_p}{\partial n^2} \right) + 2(1-\nu) \left( \frac{\partial^2 w_p}{\partial s \partial n} \right)^2 \right] d\varphi dn \quad (24)$$

where  $\nu$  is Poisson's ratio,  $D = Eh^3 / [12(1-\nu^2)]$ . method is usually used to solve the

steady-state solutions. The basic idea behind the WKB is that when the wavelengths are sufficiently short, the properties can be taken as essentially constant over the space of a wavelength. Therefore, the previously derived results can be used in this phase-integral solution, and the total phase can be written as:

$$\varphi = \omega t - \int_0^s \lambda(s) ds \quad (25)$$

Here  $W$  and  $\lambda$  in Eq. (8) and Eq. (25) are functions of  $s$  to be determined. We mainly focus on the coupling motions between fluid and BM, assuming that the vibration in  $\xi$  is the most severe, the pressure on the BM then can be written as:

$$p(s, n, 0, t) = P \left[ \eta(n) + \dots + \varepsilon^m \eta_m(n) \right] e^{i\varphi}, \quad |n| \leq \frac{1}{2} b_{BM} \quad (26)$$

where  $\varepsilon^m \eta_m(n)$  is the higher order vibration modal,  $P$  is the pressure amplitude on BM. Combine with Eq. (11), Eq. (25) and Eq. (26), using the orthogonality of different modes, then it gives:

$$P = \frac{-i\rho\omega \sum_{j=0}^{\infty} B_j A_j \cosh m_j H}{\int_{-b_{BM}/2}^{b_{BM}/2} \eta^2(n) dn} \quad (27)$$

$$\text{where } A_j = \int_{-b_{BM}/2}^{b_{BM}/2} \eta(n) \cos \left[ \frac{j\pi(n + b_{BM}/2)}{b_{BM}} \right] dn \quad (28)$$

The time-averaged kinetic energy of the fluid per unit length is expressed as:

$$T_F = \frac{1}{2\pi} \int_0^{2\pi} \int_0^H \int_{-b/2}^{b/2} \frac{1}{2} \rho (\dot{u} + \dot{v} + \dot{w})^2 dn d\xi d\varphi \quad (29)$$

For the conservative system, the total energy can be expressed as:

$$L = T_F + T_p - V \quad (30)$$

Substitute Eqs. (23), (24) and (29) into Eq. (30), the variation of  $W$  and  $\lambda$  yields the Euler-Lagrange equations:

$$\frac{\partial L}{\partial W} = 0, \quad \frac{d}{ds} \frac{\partial L}{\partial \lambda} = 0 \quad (31)$$

where the first equation of Eq.(31) gives the eikonal equation which determines the wavenumber of the wave:

$$f(\lambda) = 0 \quad (32)$$

The second equation of Eq. (31) provides the transport equation and the solution of which is the vibration amplitude of BM. It can be written as:

$$W = C \left( \frac{\partial f}{\partial \lambda} b_{BM} \right)^{-1/2} \quad (33)$$

It is usually normalize the BM amplitude with respect to that of the stapes. With the stapes motion defined as positive outward, its amplitude is:

$$\delta_{st} = - \left[ \frac{-i}{Hb\omega} \int_0^H \int_{-b/2}^{b/2} \frac{\partial \Phi}{\partial s} dn d\xi * bH \right] \Big|_{s=0} \quad (34)$$

Together with Eqs. (33) and (34), the relative amplitude of BM to the stapes can be obtained as follows:

$$\frac{w_p}{\delta_{st}} = i \left[ \left( \frac{\partial f}{\partial \lambda} \right)^{1/2} \lambda^{-1} \right]_{s=0} \left( \frac{\partial f}{\partial \lambda} \right)^{-1/2} e^{i\varphi}, \quad \varphi = \frac{\pi}{2} - \int_0^s \text{Re}(\lambda) ds \quad (35)$$

Meanwhile, in order to make our research more accurate and credible, we also established a highly physiologically accurate human ear numerical simulation model which reflecting the real spiral shape, biological material properties and lymph physiological environment of human ear, as shown in Fig. 1. The material properties and boundary conditions are chosen according to the previous literature [18-22]. The constructing process of the model can be seen in **Supplemental Material** part in detail.

Based on the analytical model and the numerical model, the vibration amplitude of BM at two frequencies 100Hz and 200Hz were calculated, as shown in Fig.2. At low frequencies (<200 Hz), the BM vibrates with equal amplitude at a regular distance along the spiral longitudinal direction, exhibiting a characteristic standing wave. The standing wave forms nodes and anti-nodes, where the amplitudes of the standing wave are maximum and minimum, respectively. As the frequency rises, the displacement of the BM increases, and the distance between adjacent anti-nodes decreases. In addition, all the points between the nodes are in phase, whereas the points on either side of a node are exactly out of phase, undergoing a phase change of  $\pi$  radians. Compared with the analytical solution, at the ends of the BM, the standing wave pattern has a variable amplitude, which may be attributed to the more accurate geometrical boundaries, material properties and lymph physiological environment of human ear numerical model. The variation of magnitudes of BM with longitudinal positions at two middle frequency 1000Hz and 2000Hz are shown in Fig. 3. With the increase of the distance from the cochlear base, there exists a transition of BM vibration from standing wave mode to traveling wave mode. The vibrating amplitude of the standing wave pattern is comparatively lower than that of the traveling wave pattern which has a notable single peak. As the frequency rises, the peak of the response curve

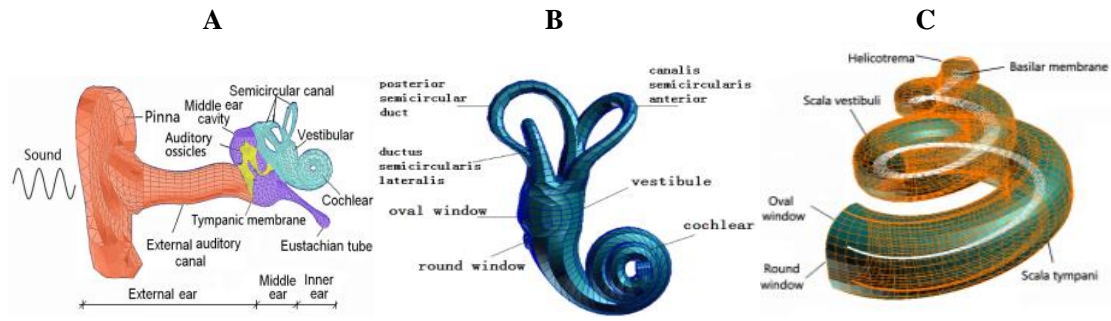


**FIG. 1 Numerical model of human ear.**(A) The whole ear. (B) The inner ear (C) The spiral-shape cochlear.

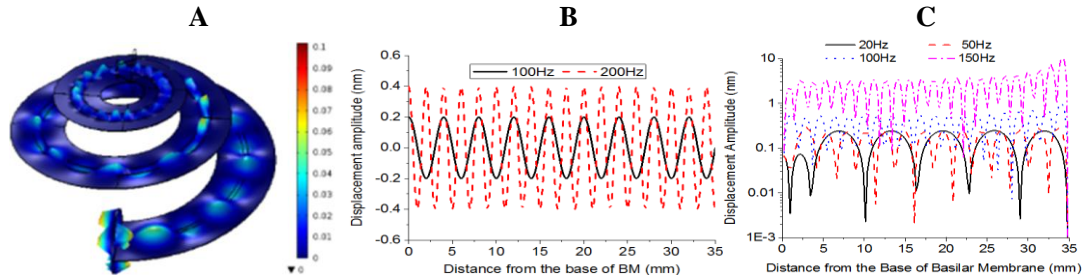


**FIG. 2 BM amplitude at low frequencies.** (A) Simulation cloud. (B) Numerical results. (C) Analytical results.

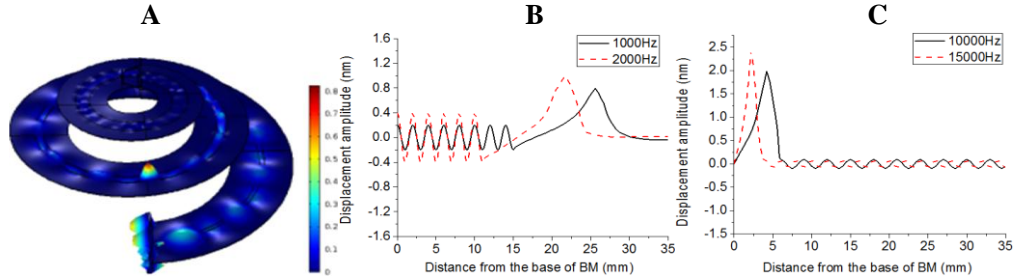


**FIG. 3 BM amplitude at high frequencies.** (A) Simulation cloud. (B) Analytical results. (C) Numerical results.

shifts from the apex to the base. After the peak, the curve declines sharply and finally tend to be flat and jugged at high frequencies. Moreover, the phase of the BM response decreases with distance from the cochlear base, which indicated that waves travels in the apical direction, that is, they form a forward traveling wave, which is exactly described by von Békésy in his traveling wave theory. At two high frequencies 10000Hz and 15000Hz, with the increase of the distance from the cochlear base, there exists a transition of BM vibration from traveling wave mode to standing wave mode. The vibrating amplitude of the standing wave pattern is also comparatively smaller than that of the traveling wave pattern.

Similar to the analytical solutions, at middle and high frequencies, the BM vibrates in a obvious traveling wave pattern. When the frequency increases to 1000Hz, the standing wave and travelling wave are concomitant, the standing wave vibration begins weakening. When the frequency is higher than 1000 Hz, the standing wave is slight, and the travelling wave vibration mode becomes dominant.

To verify the analytical and numerical models, we calculated the relationship between the magnitude of BM and the

frequency at the position 12 mm from the oval window, which were compared with the measurements [23-24], shown in Fig. 4. The results showed good agreement with both measurements with the best frequency of 3000 Hz, especially for experimental data 2.

It is worth noting that, in previous numerical models, the cochlea was assumed to be a straight shape and the lymph was assumed to be incompressible, which is not consistent with the real morphology and biomaterial properties of the cochlea [25-26]. Thus, the previous results were not consistent with the experimental measurements. Before the best frequency, the curve is not smooth but shows little pits. After the best frequency, the curve declines sharply with increasing frequency until reaching a certain high frequency, and then appears jugged. This finding is consistent with test results that have never been reflected in previous numerical models. This result may have some connection with the standing wave vibration mode.

The frequency-peak mapping curve of BM is obtained and compared with the measurements [4, 27]. We find that the simulation curve is consistent with the test curve. In addition, we predict results at very low frequencies that cannot be obtained via

the existing measurements.

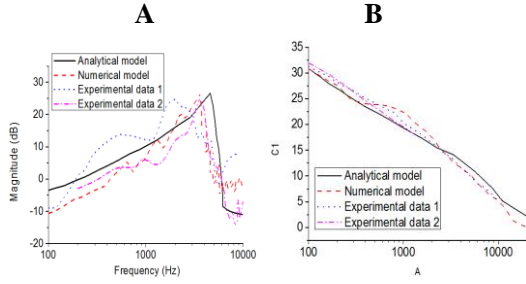


**FIG. 4 Comparison of the BM magnitude and frequency-position mapping relation (A) Displacement amplitude (B) The frequency-peak mapping curve.**

According to the above results, below 200Hz frequency, the BM mainly vibrates in a standing wave form. At frequencies between 1000Hz and 20000Hz, the travelling wave vibration becomes dominant, appearing a peak at the corresponding characteristic frequency. Due to the damping of BM and lymph, after the peak, the travelling wave sharply declines before reaching the apical end. Below 200Hz, the vibration of BM can reach the apical region. Due to the restraint of top boundary condition of cochlea, the travelling wave reaching the apex will reflect. At the same time, the reflected wave is superimposed with the travelling wave from the bottom, which makes BM occurring multiple-peak equal amplitude vibration along longitudinal direction. thus generate standing wave.

It is worth noting that, different from the previous umerical models, the material properties of the model in this paper are completely in line with physiological properties of human ear. The lymph is a compressible fluid with low viscosity. In addition, the damping of BM and lymph are introduced, which can accurately describe the dissipation characteristics of the travelling wave vibration of BM at middle and high frequencies. Thus, the traveling wave is transformed into standing wave vibration at low frequencies shown in Fig.2. The standing wave is a non-dissipating wave with arranged nodes and anti-nodes, which is an inherent vibration mode for perceiving low tones.

In fact, since the traveling wave theory was proposed by Békésy in 1960, many scientists have discovered that many experimental phenomena cannot be explained by the theory from the late period of last century by now. Kleiner [11] and Richard [12] separately pointed out that in low frequencies, BM cannot vibrate as described by the traveling wave theory and possibly vibrated within the same amplitude with multiple peaks. Meanwhile, Békésy reported that the BM would vibrate in other forms [4]. Proctor and Zandt experimentally discovered that in low frequencies, it was impossible to find

corresponding characteristic positions of single peaks of the BM vibration as depicted by traveling waves [13]. Bell discovered in his experiments that no many phases were accumulated or delayed at characteristic frequencies for vibration of the BM [28]. After experiments, Naidu and Mountain found that the test results of stiffness distribution of the BM could hardly correspond to characteristic frequencies of the membrane [29], so the vibration of BM cannot be explained by the traveling wave theory at some frequencies. Shera proposed after an experiment that otoacoustic emissions of cochlear would be explained by vibration of standing wave [30].

The standing wave vibration discovered in this paper could describe the above phenomena that unable to be explained by the traveling wave theory. We discovered that on the BM, there exhibits a standing wave which causes the BM vibrate with nodes and anti-nodes at regular distance along the longitudinal direction, appearing multiple peaks with equal amplitude (consistent with the predictions of Kleiner [12], Richard [13], and Proctor and Zandt [14]). However, the standing wave is a non-propagating wave without phase accumulation from base to the apex (coincide with Bell observations [28]). Instead, all the points between nodes are in phase, whereas the points either side of a node are exactly out of phase, undergoing a phase change of  $\pi$  radians. Compared with the single-peak traveling wave vibration in medium-high frequencies, the standing wave vibration in low-frequency is a global and severe vibration occurring entirely on the BM along the longitudinal direction. Therefore, there is no definite relation between the characteristic frequency and correspondent individual position of BM (consistent with the observations of Naidu and Mountain [29]). Although the standing wave is different from the traveling wave, there is a certain relationship between them. The standing wave is a superposition of the forward traveling wave (from base to apex) and backward traveling wave (from apex to base) that is generated by the apical boundary conditions. The standing wave vibration is a new kind of vibration mode, which is accompanied by the generation of reflecting waves (verified Shera's predictions in his experiments [30]).

As mentioned above, BM vibration data at low-frequency, which were not available through experiments, were obtained in the presented model. Meanwhile, the newly discovered vibration mode of standing waves has responded a long time puzzle of aurists and researchers, namely: why traveling wave theory could not explain many experimental observations and the behavior of the basilar membrane in low frequency vibration.

The standing wave theory has explained the coupling mechanical behaviors of low-frequency sounds in cochlea. Not single response was made in certain position on the top of BM whereas longitudinal vibration within the same amplitude is discovered along the entire BM. This new vibration mode not only enlarge sensation area of BM, but also strengthened abilities of cochlea to hear low-frequency sounds. Such inherent vibration modes in low frequencies are fundamental for cochlea to sense and encode low-frequency sounds. Besides, vibration of standing waves possibly affects the active function of cochlea, and thus explain the active phonosensitive mechanism in the cochlear which is unexplainable by the traveling wave theory.

In conclusion, the standing wave theory unveiled by the this paper is a new breakthrough for fully elucidating human ear hearing sensation mechanism. It promotes the deepening development of the human ear medicine, and may also provide theoretical basis for devising new clinical treatment of sensorineural deafness.

We would like to thank Chinese Academy of Sciences Institute of Physics for providing CT scanning based on the Synchrotron Radiation technology. This work has been supported by the National Natural Science Foundation of China(115721860, 11272200).

### References

- [1] S. G. Gwennelle, R. H. Jessfrey, Sound strategies for hearing restoration. *Science* **344**, 596-605 (2014).
- [2] J. Ashmore, Cochlear outer hair cell motility. *Physiol. Rev.* **88**, 173-210 (2008).
- [3] J. R. Colantonio, The dynein regulatory complex is required for ciliary motility and otolith biogenesis in the inner ear. *Nature* **457**, 205-209 (2009).
- [4] G. V. Békésy, *Experiments in Hearing* (McGraw-Hill, New York, 1960).
- [5] K. M. Lim, C. R. Steele, A three-dimensional nonlinear active cochlear model analyzed by the WKB numeric method, *Hear. Res.* **170**, 190-205 (2002).
- [6] F. Mammano, R. Nobili, Biophysics of the cochlea: Linear approximation. *J. Acoust. Soc. Am.* **93**, 3320-3332 (1993).
- [7] L. Robles, M. Ruggero, N. C. Rich, Two-tone distortion in the basilar membrane of the cochlea. *Nature* **349**, 413-414 (1991).
- [8] J. C. Birnholz, B. R. Benacerraf, The development of human fetal hearing. *Science* **4**, 516-518 (1983).
- [9] W. Hiroshi, S. Michiko, K. Toshimitsu, Measurement of guinea pig basilar membrane using computer-aided three-dimensional reconstruction system. *Hear. Res.* **120**, 1-6 (1998).
- [10] X. M. Zhang, R. Z. Gan, Numerical modeling of energy absorbance in normal and disordered human ears. *Hear. Res.* **301**, 146-155 (2013).
- [11] M. Kleiner, *Acoustics and Audio Technology* (J. Ross Publishing, Fort Lauderdale, ed. 3, 2011).
- [12] A. G. Richard, *Psychology: A Concise Introduction* (Worth Publishers, New York, ed.3, (2010), pp. 105-120).
- [13] R. W. Proctor, T. V. Zandt, *Human Factors in Simple and Complex Systems* (CRC Press, Boca Raton, 2008).
- [14] N. P. Cooper, W. S. Rhode, Fast traveling waves, slow traveling waves and their interactions in experimental studies of apical cochlear mechanics. *Auditory Neurosci.* **2**, 289-299 (1996).
- [15] H. Y. Lee, P. D. Raphael, J. Park, A. K. Ellerbee, B. E. Applegate, J. S. Oghalai, Noninvasive in vivo imaging reveals differences between tectorial membrane and basilar membrane traveling waves in the mouse cochlea. *PNAS* **112**, 3128-2133 (2015).
- [16] L. Robles, M. A. Ruggero, Mechanics of the mammalian cochlea, *Physiological Review* **81**, 1305-1352 (2001).
- [17] N. P. Cooper, W. S. Rhode, Nonlinear mechanics at the apex of the guinea-pig cochlea. *Hear. Res.* **82**, 225-243 (1995).
- [18] W. Yao, J. Ma, B. Hu, Numerical model on sound-solid coupling in human ear and study on sound pressure of tympanic membrane. *Math. Probl. Eng.* **3**, 356-362 (2011).
- [19] W. Yao, B. Li, X. Huang, C. Guo, X. Luo, W. Zhou, M. Duan, Restoring hearing using total ossicular replacement prostheses-analysis of 3D numerical model. *Acta. Otolaryngol.* **132**, 152-159 (2012).
- [20] W. Yao, C. Guo, X. Luo, Study on effects of partial ossicular replacement prosthese with different materials on hearing restoration. *J. Mater. Sci. : Mater. Med.* **24**, 515-522 (2013).
- [21] W. Yao, J. Ma, X. Huang, Numerical simulation of the human ear and the dynamic analysis of the middle ear sound transmission. *J. Instrum.* **8**, 1-13 (2013).
- [22] W. Yao, X. Huang, L. Fu, Transmitting vibration of artificial ossicle. *Int. J. Nonlin. Sci. Num.* **9**, 131-139 (2008).
- [23] S. Stenfelt, S. Puria, N. Hato, R. L. Goode, Basilar membrane and osseous spiral lamina motion in human cadavers with air and bone conduction stimuli. *Hear. Res.* **181**, 131-143 (2004).
- [24] T. Gundersen, O. Skarstein, T. Sikkeland, A study of the vibration of the basilar membrane in human temporal bone preparations by the use of the Mossbauer effect. *Acta. Otolaryngol.* **86**, 225-257 (1978).
- [25] S. Liu, R. D. White, Orthotropic material properties of the gerbil basilar membrane. *J. Acoust. Soc. Am.* **123**, 2160-2171 (2008).
- [26] A. Cho, Math clears up an inner-ear mystery: spiral shape pumps up the bass. *Science* **24**, 1087 (2006).
- [27] D. D. Greenwood, A cochlear frequency-position function for several species--29 years later. *J. Acoust. Soc. Am.* **87**, 2592-2605 (1990).
- [28] A. Bell, Hearing: traveling wave or resonance?. *Plos Biol.* **2**, 337 (2004).
- [29] R. C. Naidu, D. C. Mountain, Measurements of the stiffness map challenge: a basic tenet of cochlear theories. *Hear. Res.* **124**, 124-131 (1998).
- [30] C. A. Shera, Mammalian spontaneous otoacoustic emissions are amplitude stabilized cochlear standing waves. *J. Acoust. Soc. Am.* **114**, 244-262 (2003).